Applied Energy 379 (2025) 124947

Contents lists available at ScienceDirect

Applied Energy

journal homepage: www.elsevier.com/locate/apenergy

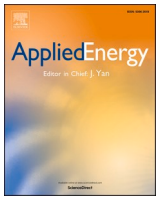

Cooling demand reduction with nighttime natural ventilation to cool internal thermal mass under harmonic design-day weather conditions

Mingtong Li [a], Xiong Shen [b], Wentao Wu [a,*], Kristen Cetin [c], Finn Mcintyre [d], Liangzhu Wang [e], Lixing Ding [f], Daniel Bishop [a], Larry Bellamy [a], Meng Liu [g]

[a] Department of Civil and Natural Resources Engineering, University of Canterbury, New Zealand
[b] Department of Building Environment and Energy Application, Tianjin University, China
[c] Department of Civil and Environmental Engineering, Michigan State University, East Lansing, MI, USA
[d] Department of Mechanical Engineering, University of Canterbury, New Zealand
[e] Centre for Zero Energy Building Studies, Department of Building, Civil and Environmental Engineering, Concordia University, Canada
[f] College of Mechanical and Electrical Engineering, Zhongkai University of Agriculture and Engineering, Guangzhou, China
[g] National Centre for International Research of Low-Carbon and Green Buildings (Ministry of Science and Technology), Chongqing University, China

HIGHLIGHTS

- Develop a design framework for nighttime natural cooling of internal thermal mass.
- Optimum thickness for internal thermal mass is between 28 and 45 mm.
- Internal mass with lightweight wall achieves peak cooling load reduction by 35.9 %.
- The belt between Tropic of Cancer and 60°N suitable for using internal thermal mass.
- Annual cooling demand reduction can reach 6.67 kWh/m^2 in desert climate zones.

ARTICLE INFO

Keywords:
Night cooling
Passive building technique
Energy efficiency
Building simulation
Climate zones

ABSTRACT

Cooling demand is steadily increasing across different climate zones due to global warming. A potential solution for cooling demand reduction is applying nighttime natural ventilation to cool internal thermal mass. However, a simplified and accurate modelling framework to assess the technique is still missing. The goal of the study is to build that framework integrated with a validated internal thermal mass model and apply the framework to quantify the cooling demand reduction potential in a space with different thermal mass and envelope configurations and in different climate zones. Results show that using Granite as internal thermal mass is three times more effective than concrete to reduce peak cooling load. Adding too much internal thermal mass can create adverse effects on cooling load reduction. The optimum thickness of internal thermal mass is between 28 and 45 mm. Envelope construction also has an influence on the performance of nighttime cooling. Applying the technique in buildings with lightweight structures reduces peak cooling load by 35.9% more than heavyweight structures. As heavyweight structures delay the release of the daily absorbed heat and cause higher indoor air temperatures at night. The two belts between the Tropic of Cancer and 60 degrees north latitude, and between the Tropic of Capricorn and 45 degrees south latitude are suitable for nighttime natural ventilation of internal thermal mass, achieving the annual cooling demand reduction above 1.25 kWh m^{-2}. In Dessert climate zones, the technique exhibits an extraordinary potential to reduce cooling demand, up to 6.67 kWh m^{-2} per year.

1. Introduction

Cooling demand is expected to grow at more than 3% a year for the next 30 years due to global warming [1]. Even for a heating-demand-dominant country like New Zealand, it is projected that the average annual cooling demand in Auckland will increase from 9.63 kWh m^{-2} to 16.05 kWh m^{-2} by 2025 under the Representative Concentration Pathways 4.5 scenario [2]. The increasing cooling demand would further intensify electricity demand, especially during extreme high-

* Corresponding author.
E-mail address: wentao.wu@canterbury.ac.nz (W. Wu).

https://doi.org/10.1016/j.apenergy.2024.124947
Received 5 July 2024; Received in revised form 26 October 2024; Accepted 15 November 2024
Available online 26 November 2024

Nomenclature

Abbreviations

IM	InternalMass
ZCM	ZoneCapacitanceMultiplier
ACH	Air Change rate per Hour
DBR	Dry Bulb temperature Range
CTF	Conduction Transfer Function
SHGC	Solar Heat Gain Coefficient

Variables

$\dot{Q}$	Cooling load (W)
T_s	Top surface temperature of the thermal mass (K)
T_r	Indoor air temperature (K)
T_o	Outdoor air temperature (K)
V	Volume of the room (m^3)
q	Heat gain (W)
A	Floor area (m^2)
A_{op}	Window opening area (m^2)
D_h	Hydraulic diameter of the floor (m)
t	Calculating hour
h	Convection heat transfer coefficient (W m^{-2} k^{-1})
h_{st}	Useful stack effect height for airing (m)
C_{wind}	0.001 (m^{-1})
C_{st}	0.0035 (m K^{-1} s^{-2})
E	Solar radiation (W m^{-2})
u_0	Wind speed at the reference site (m s^{-1})

Greek symbols

ρ	Density of mass (kg m^{-3})
λ	Thermal conductivity of internal thermal mass (W m^{-1} K^{-1})
ρ_a	Air density (kg m^{-3})
$\rho_{a,site}$	Air density at reference site (kg m^{-3})

Subscript

cl	Cooling demand
e	Conductive cooling load /heat gain through exterior walls and roofs
s	Cooling load /heat gain due to solar heat gain through windows
g	Conduction cooling load due to windows
i	Cooling load due to internal heat gains
inf	Cooling load due to infiltration
itm	Cooling load reduction due to the presence of internal thermal mass
ext	Heat gains due to External walls and roofs

temperature weather events [3]. In July 2023, after several weeks of temperatures above 43°C in Arizona, the peak electricity demand reached 8191 MW that was 531 MW higher than the prior record [4]. The recorded electricity peak was mainly attributed to active space cooling.

Shifting and shaving cooling demand by using passive design is of a great potential to alleviate the strain on electricity grid [5]. Properly utilising building materials can help to shift, and shave cooling load by absorbing and releasing heat at a time lag [6]. The product of building material density and specific heat capacity is called thermal mass [7]. The performance of thermal mass on thermal load management may vary with its positions [8]. In this study, thermal mass on floor and exposed to indoor air is defined as internal thermal mass, whereas thermal mass on wall and exposed to outdoor air is designated as external thermal mass. In temperate climates, experiments in two real-scale single-family houses show that replacing lightweight walls with cellular concrete of high external thermal mass can reduce the cooling demand by 67%–75% with cooling setpoint temperatures between 25°C and 26°C [9]. In cold-humid climates, adding a 100-mm thick concrete layer as external thermal mass can achieve energy consumption reduction of 20% and 75%, respectively, during hot and transitional seasons [10]. In hot-desert climate, substituting hollow red bricks in external walls with stones of high thermal mass can reduce cooling demand up to 72% [11]. However, some studies point out that external thermal mass could have limited or adverse effects on building energy use [6]. A study in hot climates shows that the energy consumption reduction by using high thermal mass is negligible, only 3 kWh m^{-2} over the course of year [12]. Purely increasing external thermal mass results in 17.5% increase in overheating hours in a Chinese city – Kunming, which has a temperate climate [13]. The controversial conclusions on the capability of external thermal mass to manage cooling load is related to the type of dominant thermal loads, buildings, etc. The influence factors are summarised in Table A1 in Appendix A. Residential buildings are mostly occupied during night and external thermal mass releasing daily absorbed heat during the night will increase the cooling demand. If the dominant load in a space is people, external thermal mass functions to hinder the heat dissipation through envelopes and results in the increase of cooling demand.

Internal thermal mass is less dependent on dominant load and building type. It may provide stable performance on cooling load reduction and indoor air temperature management. For example, in a cloud-shading scenario, only using internal thermal mass can limit indoor temperature increase to 2°C in the first 50 min when cooling system is switched off [14]. A numerical study shows that internal thermal mass can lead to a 40% increase in the building time constant (the rate of influence of outdoor temperature variations on the indoor thermal conditions) and thermal delay (the time needed for the mean indoor temperature to change by a specified amount under a specified thermal load) [15]. The presence of internal thermal mass in buildings with lightweight structures can increase the time constant by 42% and the energy flexibility, the ability for the building to minimise the energy usage during high price periods, by up to 21% [16]. However, these studies did not consider how the configuration of envelopes [17], e.g., light- or heavyweight exterior walls and roofs, influences the thermal performance of the internal thermal mass.

Using only internal thermal mass has limited capacity to reduce cooling demand. A strategy to enhance the performance of internal thermal mass to reduce cooling load is to apply nighttime mechanical ventilation. A study shows that the maximum heat removed from the internal thermal mass during the period of 10-h nighttime ventilation, is 19.1 kWh m^{-2} per year with an annual electricity energy consumption of 15.2 kWh m^{-2} by mechanical fans [18]. The mechanical fan energy use for nighttime ventilation may be depleted by natural ventilation [19]. Research has shown that employing nighttime natural ventilation significantly enhances the release of accumulated heat in thermal mass, thereby creating heat sinks in the following day to reduce cooling load [20]. A study using computational fluid dynamics modelling reveals that application of nighttime natural ventilation to cool a concrete slab as internal thermal mass reduces daily peak air temperature by 6°C [21]. In a non-residential building, pre-cooling the structure with natural ventilation overnight can reduce the average cooling load by 27% during summer days [22]. Even during heatwave conditions, overnight natural ventilation of a nearly-zero building in Belgium mitigates overheating up to 0.50°C [23]. Even in a hot summer, the application of nighttime natural ventilation can achieve 15.3% energy savings in ultra-low energy buildings in Shenyang, China [24]. Most state-of-the-art

studies on nighttime natural ventilation focus on the combined effect with external thermal mass [25] [26] [27] [28]. Work on nighttime cooling of internal thermal mass is limited as it requires simplified, accurate, and fast design tools [29].

Whole building energy simulation program – EnergyPlus is a popular tool for cooling load calculation involving thermal mass and natural ventilation [30]. There are two approaches to model internal thermal mass in EnergyPlus: InternalMass (IM) and ZoneCapacitanceMultiplier (ZCM). The ZCM method adds the effective storage capacity of thermal mass to the thermal capacitance of the zone air by a multiplier. It indicates adding more and more internal thermal mass would lead to a larger and larger multiplier as well as higher and higher efficiency of internal thermal mass to regulate indoor air temperature. This is unlikely if the internal thermal mass is concrete slab as the temperature variation within the thermal mass becomes smaller with increasing thickness, as demonstrated in the work [18]. The IM method creates an internal object with defined materials and surface area. The internal object will modify the zone air heat balance. The IM method shows a significant deviation with measurement [14]. Besides whole building energy program, many parametric models have been developed for thermal mass [18]. A second-order heat balance model has been developed for evaluating the impact of external thermal mass on indoor air temperature [31]. An effective thermal capacity, like the ZCM method used in EnergyPlus, is added to indoor air to include the effect of the thermal mass in the external wall. The heat transfer between the inner surface of the external wall and the indoor air is characterised by a temperature elastic coefficient, defined as the derivative of indoor air temperature to the inner surface temperature. This model is based on constant room ventilation rate and not suitable for nighttime natural ventilation with time-varied ventilation rates. A low-parameter linear model has been developed to assess energy flexibility potential of thermal mass [32]. This first order model bases on the transfer function method and might not be suitable for integrating natural ventilation and internal thermal mass. Another common feature of these simplified models is that they do not consider dimensional effect of internal thermal mass due to the lumped parameter assumption [33].

Collectively, a design tool for the technique using nighttime natural ventilation of internal thermal mass is missing; what is the optimum thickness of specific materials for internal thermal mass to maximize the cooling load reduction potential? How would the light- or heavy-weight external structural configuration affect the performance of the technique? Which climate zones are the technique suitable for?

The primary goal of this study is to develop a modelling framework to quantify the potential of nighttime natural ventilation of internal thermal mass to reduce cooling load under different climates and envelope configurations. Specifically, we integrate an internal thermal mass model into heat balance equations that rely on the conventional radiant time series method for cooling load determination [34] and the ISO EN 16798–7 model for natural ventilation calculation [35]. Comparing to previous work [18], which is based on a constant convection heat transfer coefficient over the internal thermal mass, this study develops a new model that uses hourly varied convection heat transfer coefficients and is suitable for nighttime natural ventilation scenarios. The thermal mass model takes hourly varied indoor air temperature and convection heat transfer coefficients as inputs. The hourly input values link the thermal mass model with the natural ventilation model. To validate the thermal mass model, experiments in a climate chamber were carried out to record the temperature history in the thermal mass on the floor slab. The framework is applied to study the impact of light- and heavyweight envelope construction on the performance of nighttime natural ventilation of internal thermal mass. Finally, the applicability of the above strategy is explored in 1871 worldwide cities in different climate zones. This study is expected to provide a simple building technique to reduce the steadily increasing cooling demand due to global warming.

2. Materials and methods

2.1. Experiment setup

The climate chamber (Fig. 1) located inside a laboratory has a size of 3.68 m × 2.44 m × 2.56 m. The roof and walls are made of OSB Formance Panels with an overall U value of 0.38 W m^{-2} K^{-1}. The floor is made of black sand paver as internal thermal mass and fully insulated with polystyrene to minimise heat loss to the ground. The paver block has a size of 300 mm × 300 mm × 500 mm, and 60 pavers in total were installed to cover the entire floor. The paver has a density (ρ) of 2034 kg m^{-1}, a specific heat capacity (c) of 440 J kg^{-1} K^{-1}, and a thermal conductivity (λ) of 0.4 W m^{-1} K^{-1}. Paver is chosen due to material availability, low cost, easy installation, and demolishment. The material also well satisfies the model validation purpose.

A heat pump is used to generate time-variant temperature and ventilation rates to mimic time-variant indoor air conditions. The type of the heat pump is MODEL MPPD27H (Midea®) with a heating capacity of 2.80 kW. The heat pump has four fan modes to adjust ventilation rates. Eight thermocouples of type-12K are used to measure air and solid surface temperatures. One thermal couple is located outside the chamber to monitor the air temperature in the laboratory. One thermal couple is placed 0.20 m above the paver to record the air temperature in the chamber. Three thermal couples are attached to the top and bottom surface, respectively, to measure the temperatures on the thermal mass. The air speed at 0.20 m above the internal thermal mass is measured to derive convection heat transfer coefficients. The anemometer is Miniature hotwire probe (DANTEC Dynamics®) and has an accuracy of ±0.5%.

The main purpose of the chamber experiment is to validate the internal thermal mass model. Although the thermal mass model is used for cooling load management in this study, the model itself has a wider application describing heat transfer due to time-variant free stream temperatures and convection heat transfer coefficients. Therefore, measurements in this study are carried out under heating scenarios but the validation is also valid for cooling scenarios. Two measurements were carried out for 16 and 8 h, respectively. The experiments are manually operated, which involves opening the door. During the two measurement periods, the ambient temperature outside the chamber was consistently around 18°C. Before each measurement, the chamber is closed for 3 days to allow the thermal mass and the chamber air to achieve equilibrium. When the measurements are initiated, the heat pump is set to 30°C. In the first experiment, once the chamber air temperature reaches 30°C, the chamber door is opened to switch the heat pump off. When the top and bottom surface temperature of the thermal mass converge towards the same value, the heat pump is activated again. The on and off activity is to vary convection heat transfer coefficients on purpose. During the heat pump operation period, the air movement above floor is driven by fan of the heat pump and corresponds to forced convection, whereas during the fan-off period, it corresponds to natural convection. However, opening chamber door causes fluctuations in the inside air temperature. Hence, in the second measurement, the chamber door is closed during entire measurement period and the heat pump is kept on and off according to its setpoint temperature. For both measurements, data from the anemometer and the thermal couples are recorded into a computer at a time interval of 1 min.

2.2. Numerical simulations for model comparison

Numerical method using the laplacianFoam solver in open-source code - OpenFoam 8 is conducted for comparison between analytical and numerical solutions. The laplacianFoam can be used to solve the transient heat transfer in the internal thermal mass (Eq. B1 in Appendix B). The dimensions and properties of the internal thermal mass, the room air temperatures and the convection heat transfer coefficients for boundary conditions are the same as conditions in the above

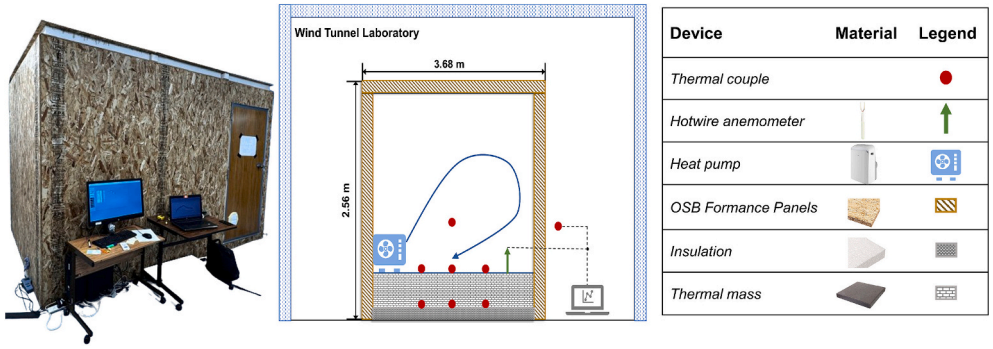

Fig. 1. Experiment chamber with indication of sensor locations.

experiments. The internal thermal mass is discretised into 100 cells along the thickness. The Laplacian term is discretised by Gauss Linear corrected scheme. The time derivative is discretised with Euler scheme. The time step is chosen as 1 s to satisfy the convergence conditions specified in the literature [18].

2.3. The mathematical modelling framework

The nighttime natural ventilation of internal thermal mass refers to a system presented in the work [18] by replacing nighttime mechanical ventilation with natural ventilation. To develop a new model for nighttime natural ventilation of internal thermal mass, the following assumptions were made:

1) During the daytime, the room is air conditioned to maintain a constant set point temperature of 23.3°C.

2) During nighttime natural ventilation, the room air temperature is uniformly varied. If the air-conditioning system is not used during the daytime, the equation for nighttime ventilation (Eq. 2) is applied to both day- and nighttime heat balance.

3) Convection is considered as dominant heat exchange between the internal thermal mass and the indoor air. Longwave radiation is not accounted for at this stage.

The heat balance for a room with such a system has been described by Yang and Li [36]:

$$\text{Daytime } \dot{Q}_{cl} + \dot{Q}_e + \dot{Q}_g + \dot{Q}_s + \dot{Q}_i + \dot{Q}_{inf} + \dot{Q}_{itm} = 0 \tag{1}$$

$$\text{Nighttime } \rho_a c_a ACH(T_o - T_r)V + \dot{Q}_{itm} + \dot{Q}_e + \dot{Q}_{inf} + \dot{Q}_g + \dot{Q}_i = 0 \tag{2}$$

Eq. (1) describes the heat balance of a room during the day with an air conditioning system to maintain a constant setpoint temperature. The cooling loads through walls, roofs, windows, and infiltration are determined by the conventional radiant time series method [37]. At the initial moment of calculation, it is assumed that the room is at a uniform temperature of 23.3°C, and the bottom of the room's floor is well insulated. The cooling load reduction due to internal thermal mass is calculated as,

$$\dot{Q}_{itm} = hA(T_s - T_r) \tag{3}$$

The Beausoleil Morrison correlations [38] and Rui Guo correlation [39] are chosen to calculate convention heat transfer coefficients. When the floor surface temperature is lower than the room air temperature, Eq. (4) is applied to consider the thermally stable flow condition above the floor. Vice versa, Eq. (5) is applied to consider the thermally unstable flow condition.

$$\text{Daytime } h = 0.31 + 0.34ACH^{0.8} \tag{4}$$

Nighttime

$$\begin{cases} h^3 = \left[0.6\left(\dfrac{|T_s - T_r|}{D_h}\right)^{\frac{1}{5}}\right]^3 + \left[\dfrac{T_s - T_o}{|T_s - T_r|}\left(0.159 + 0.116ACH^{0.8}\right)\right]^3 & T_s < T_r \\ h^3 = \left\{\left[1.4\left(\dfrac{|T_s - T_r|}{D_h}\right)^{\frac{1}{4}}\right]^6 + \left[1.63|T_s - T_r|^{\frac{1}{3}}\right]^6\right\}^{\frac{3}{6}} + \left[\dfrac{T_s - T_o}{|T_s - T_r|}\left(0.159 + 0.116ACH^{0.8}\right)\right]^3 & T_s > T_r \end{cases} \tag{5}$$

The daytime ACH is assumed to be constant. The nighttime ACH will be explained in Eq. (9). The top surface temperature T_s of the internal thermal mass is calculated with the formula (B7). The thermal mass formula takes h and T_r as input and can be used to calculate the temperature at any depth (L) in the thermal mass. The formula is essentially an analytical solution derived for the one-dimensional heat conduction equation (Fig. 2) with Robin boundary condition on the top surface and adiabatic boundary condition the bottom surface. The detailed derivation is given in Appendix B. The top surface temperature T_s is re-organised for hourly data input:

$$T_s(t) = T_r(0)\sum_{n=1}^{5}\varphi_n(t)cos\beta_n + T_r(0) \tag{6}$$

$$\varphi_n(t) = \frac{1}{W4_n(t)}\left\{\sum_{j=0}^{t-1} e^{-\sum_{i=j}^{t-1} W2_n(i+1)\frac{\lambda}{\rho cL^2}} G_n(j) + G_n(t)\right\} \tag{7}$$

$$G_n(j) = A_n(j+1)\left\{\frac{W1_n(j+1)}{W2_n(j+1)}\left[1 - e^{-W2_n(j+1)\frac{\lambda}{\rho cL^2}}\right] - W3_n(j+1)e^{-W2_n(j+1)\frac{\lambda}{\rho cL^2}}\right\} \tag{8}$$

A detailed description of the model coefficients can be found in Appendix B.

Eq. (2) describes the variation of the indoor air temperature in the room during the night with natural ventilation. Nighttime ACH is calculated by Eq. (9) introduced by ISO Standard EN 16798–7:2017 [40]. The simple direct calculation model computes the ventilation rates from the maximum contribution coming from wind or stack effect. This

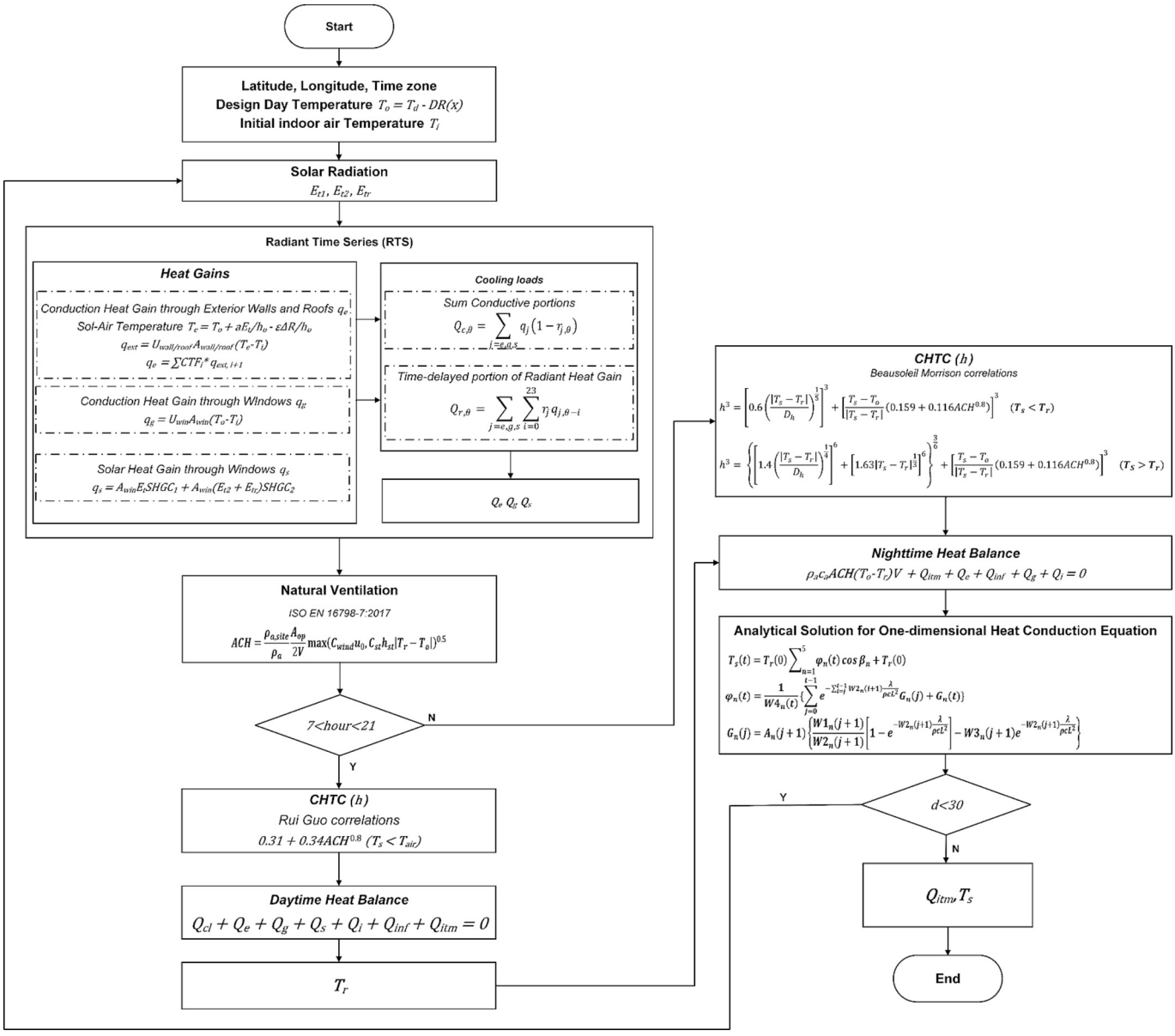

Fig. 2. Flow chart of the mathematical modelling framework.

equation has been validated in literature [35,41] and is well suited for quantifying the single-sided natural ventilation rates in this study.

$$ACH = \frac{\rho_{a,site}}{\rho_a}\frac{A_{op}}{2V}max\left(C_{wind}u_0^2, C_{st}h_{st}|T_r - T_o|\right)^{0.5} \quad (9)$$

The primary goal of this study is to understand the cooling load reduction by designing nighttime natural ventilation and internal thermal mass. Therefore, the outdoor air temperature T_o is chosen as the design-day temperature of different months. The determination of the design-day outdoor air temperature can be found in [35]. The entire framework is illustrated by the diagram in Fig. 2 and coded in Julia.

2.4. Case-study room

In this study, a case-study room [37] with a size of 9.14 m × 9.14 m × 3.66 m is chosen to represent a single zone, e.g., an office, in a building. The room has a roof and an external wall with four identical windows (1.52 m × 1.22 m). The external wall is designated to face south and north, for northern and southern hemisphere, respectively. All configurations of wall and roof assemblies listed in Table 16, 17 and 18 in Chapter 18 of ASHRAE Handbook 2021 [42] are tested in this study to understand the impact of envelope construction on the performance of cooling load reduction by using nighttime natural ventilation of internal thermal mass. The type of windows specified as number 13 in Table 10, Chapter 15 of the ASHRAE Handbook 2021 [42]. The internal thermal mass is located on the floor with its bottom surface insulated. Six materials [43] are selected as internal thermal mass and their physical properties are given in Table 1. All the other surfaces of the room are

Table 1
Thermal properties of internal thermal mass materials.

	ρ (kg m^{-3})	c (kJ kg^{-1} K^{-1})	λ (W m^{-1} K^{-1})
Brick	1600	0.84	1.20
Ceramic	2000	0.90	2.00
Clay Sheet	1900	0.84	0.85
Concrete	2240	1.13	1.10
Granite	2650	0.90	2.90
Marble	2500	0.88	2.00

assumed to be internal partitions that do not participate cooling load calculations. There are 10 occupants working in the office from 8 am to 5 pm and generating 750 W heat gains. The heat gain of equipment is 180 W from 8 am to 5 pm and 900 W from 5 am to 8 pm. The heat gain of lights is 270 W from 8 am to 5 pm and 1350 W from 5 pm to 8 am. The setpoint temperature for cooling is 23.3°C. The room is predetermined to locate on the top floor of the building, configurated with a roof and an external wall containing four identical windows resulting in relatively higher cooling load. If the room were located on a middle floor without a roof, the cooling load may be lower, and the energy-saving performance of the internal thermal mass would be more effective. Conversely, if the room located in the corner of the top floor, the energy-saving performance of the internal thermal mass would be decreased due to potential higher cooling load. Therefore, the case-study room is assumed to represent a general case.

2.5. Climate data

Daily outdoor temperature profiles are generated using the monthly design dry bulb temperature and the mean daily temperature range, as provided by ASHRAE [44]. 1871 worldwide cities have been selected based on climate zones, population density, and the continent. Climate zones are classified according to Köppen-Geiger classification system, which primarily categorises global climate types into four groups: Tropical, Arid, Temperate, and Cold, excluding Polar regions due to their low population density and incomplete weather data. Tropical and Arid Desert climates mainly comprise Latin America, Africa, and Australia, where there is a lack of weather stations in certain African and Latin American regions [45]. Therefore, limited cities are chosen from these regions [44]. Due to the large sample size in the ASHRAE Climatic Design Conditions [44], which includes data from most meteorological stations worldwide, uniform sampling is employed to select regions. One city is chosen out of every ten cities in the list of the ASHRAE Climatic Design Conditions. In countries where the number of meteorological stations is less than five, the first station is manually selected to ensure the completeness of the national samples. As shown in Fig. 3, the obtained weather and site data is written into a spreadsheet. The weather data tables are loaded into the modelling framework in Julia for iterative calculations of energy data. This data is then used for visualization and factor analysis.

2.6. Parameters to evaluate the performance of internal thermal mass

During daytime, the internal thermal mass absorbs heat from the indoor air and the process is termed as “heat absorbed from room air”. During nighttime, the natural ventilation removes the heat from the internal thermal mass and the process is termed as “heat released into room air”. The amount of internal thermal mass used to reduce indoor cooling energy demand during peak times is referred to “peak cooling load reduction”. Additionally, the dry bulb temperature range is abbreviated to DBR.

The normalized mean bias error (NMBE) and coefficient of variation of the root mean square error Cv(RMSE) [46] are further used to quantify the relative errors between the experiments and the model.

$$NMBE = \frac{1}{n}\frac{\sum_{i=1}^{n}(S_i - M_i)}{\overline{M_i}} \times 100\% \tag{10}$$

$$\mathrm{Cv(RMSE)} = \frac{\sqrt{\frac{1}{n}\sum_{i=1}^{n}(S_i - M_i)^2}}{\overline{M_i}} \times 100\% \tag{11}$$

where S_i is the measurement data from experiment, M_i is the simulation data from numerical model.

3. Results and discussion

3.1. Model validation

This simulation examined the temperature changes over time in the same paver as the experiment. In experiment 1 (Fig. 4a), the deviation

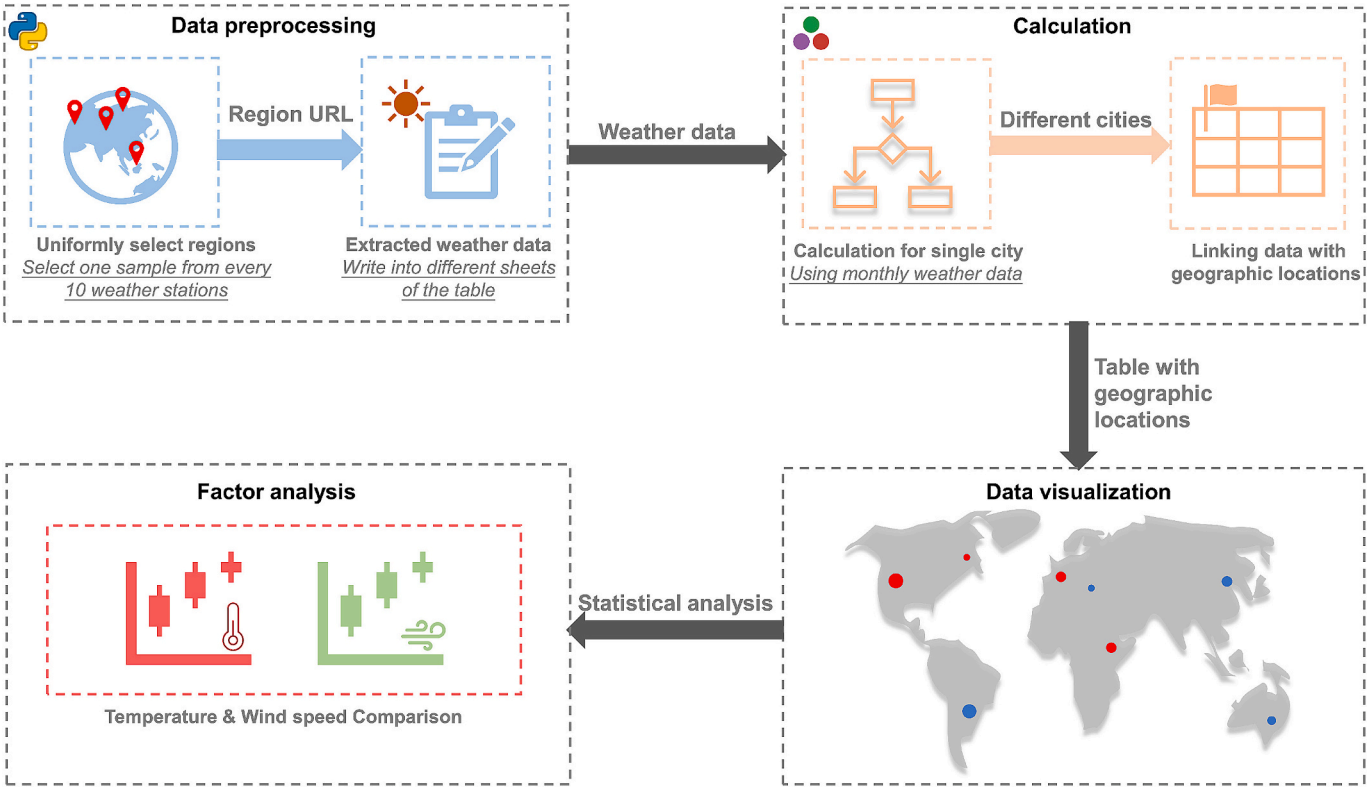

Fig. 3. Schematic diagram of weather data extraction.

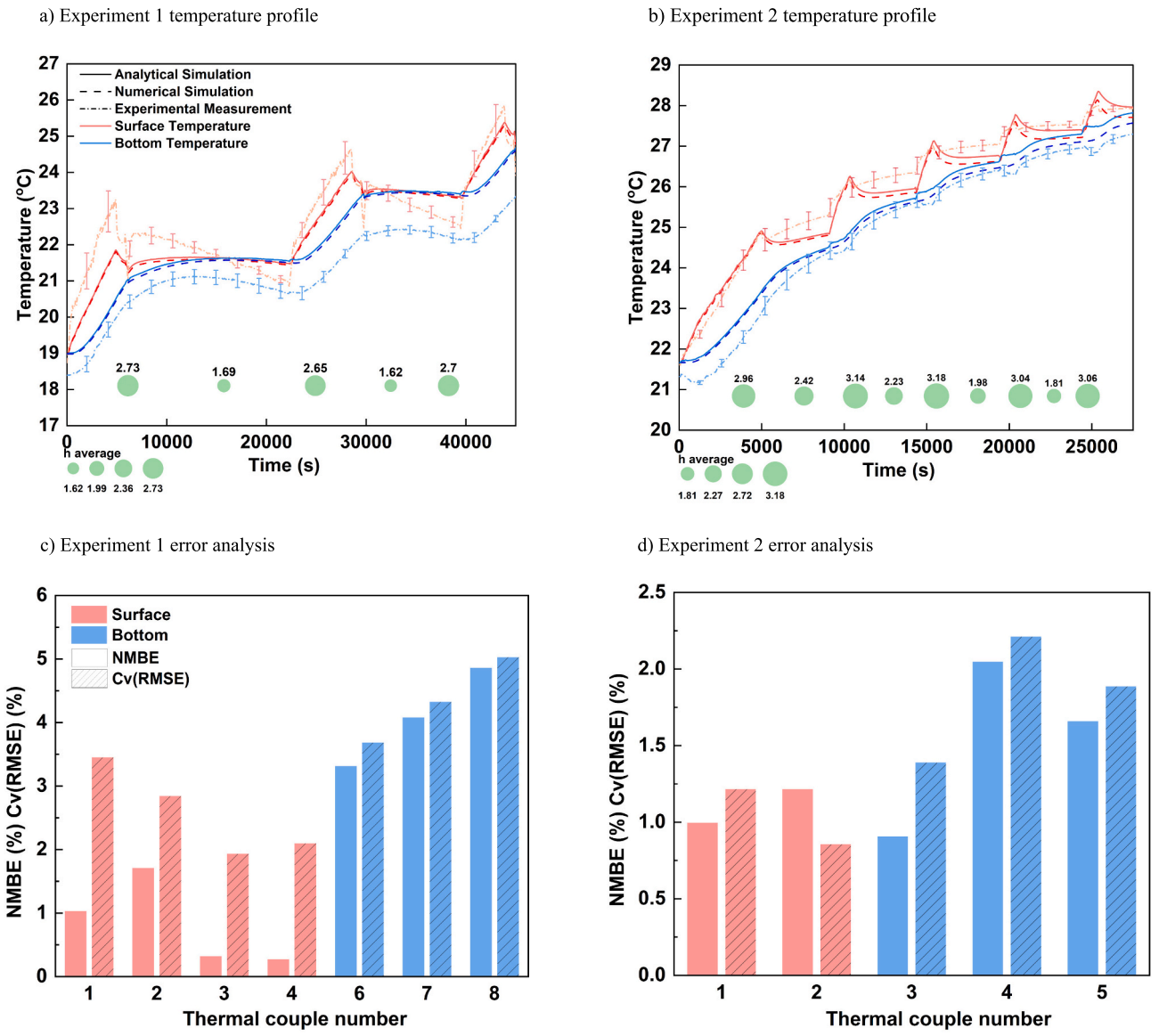

Fig. 4. Temperature history on the top and bottom surface of the internal thermal mass. Green bubbles show the average convection heat transfer coefficient during each heat pump on and off period; solid lines denote temperatures calculated from analytical model; dash lines denote numerical simulation results; dash dot lines are for experiments. Red colour denotes temperatures on the surface of the internal thermal mass; blue colour is for bottom. (For interpretation of the references to colour in this figure legend, the reader is referred to the web version of this article.)

between the top surface temperatures measured by six thermal couples is less than 1.1°C, which indicates the heat transfer in the internal thermal mass is one-dimensional. When the heat pump is on, the measured top surface temperatures increase from 18.6 ± 0.1°C to 23.6 ± 0.5°C. The top surface temperature calculated by the model increases till 26.1°C showing a maximum discrepancy of 1°C. A sudden drop in the top surface temperatures is due to door opening. The analytical model can predict the sudden temperature change to a certain extent. When the heat pump is off, the measured top surface temperature decreases to 20.8°C and the top surface temperature calculated by the model remains 21.5°C. The model does not capture the decreasing trend in the measurement. This is probably because the free convection heat transfer coefficients are not well estimated when the air speed above the floor is extremely low. For bottom surface temperatures, the model predicts well the temperature variation trend as that in the measurement but shows a consistent deviation that scales to 2°C after two cycles of heat pump operation. It seems that door opening causing sudden temperature variations and exacerbates the relative errors between experiments and the model. Maximum NMBE for top and bottom surface temperature is 5.5% and 4.5%, respectively. Maximum Cv(RMSE) is 6.9% and 4.7%,

Table 2
Errors between analytical and numerical model (%).

	Simulation 1 surface	Simulation 1 bottom	Simulation 2 surface	Simulation 2 bottom
NMBE	0.25	0.29	0.49	0.59
Cv(RMSE)	0.27	0.28	0.59	0.96

respectively, for top and bottom surface temperature. The small values indicate good agreement between experiments and the model. To reduce the error caused by door opening, experiment 2 (Fig. 4b) is run without opening the door. After one cycle of heat pump operation, the deviation between the predicted and measured temperatures is smaller than 0.5°C for both top and bottom surface of the internal thermal mass. The NMBE value is reduced to 1.2% for top surface and 2.1% for bottom surface. Cv (RMSE) is reduced to 0.9% for top surface and 2.0% for bottom surface.

Both the maximum NMBE and Cv(RMSE) shown in Table 2 is lower than 1%, showing a good match between the numerical simulation and the analytical model. The good match reveals that sudden temperature changes and estimation of free convection heat transfer coefficients in the experiments are the major sources of errors in NMBE and Cv(RMSE) between experiments and models.

3.2. Optimum materials and thickness

The peak cooling load reduction potential (Fig. 5a) of a specific material used as internal thermal mass is illustrated for only one location - Taos, New Mexico, in July, with the building type set as lightweight. For different materials, if one material (e.g., granite) shows better performance comparing to other materials in one location (e.g., Taos), it is expected to perform better in other locations as well. But for the same material, its potential on cooling load reduction varies with climates. As part of building components, identifying the performance differences between materials is more crucial than their absolute values. This focus allows for the selection of materials that maximize the efficiency of passive cooling. Among the six tested materials, concrete shows the lowest peaking cooling load reduction of 0.37 W m^{-2}. But concrete has a large thermal mass (ρc) of 2531 kJ m^{-3} K^{-1} and requires a lower volume of material. Clay sheet has a small thermal mass 1590 kJ m^{-3} K^{-1} and shows a low peak cooling load reduction, but still two times more effective than concrete. Brick has a small thermal mass of 1344 kJ m^{-3} K^{-1} but shows a load reduction three times more than concrete. Concrete, clay, and brick have low thermal conductivities and are not optimum materials for nighttime natural ventilation of internal thermal mass to reduce peak cooling load in the following day. Granite, ceramic, and marble exhibit significantly larger thermal masses, with values of 1.77, 1.34, and 1.64 respectively, compared to the thermal mass of brick. Additionally, granite, ceramic, and marble decrease peak cooling load by approximately 3.3, 3.4 and 3.0 times more than concrete, respectively. Granite, ceramic and marble also have a high thermal conductivity and are good candidates for nighttime natural ventilative cooling of internal thermal mass.

To provide a comprehensive graph to aid the selection of materials, a sensitivity analysis was conducted on λ and thermal diffusivity ($\alpha = \lambda/\rho c$). One hundred data points are uniformly sampled within the ranges of λ (0.1–3.5 W m^{-2} K^{-1}) and ρc (100–5000 kJ m^{-3} K^{-1}), resulting in the analysis of 10,000 potential materials. The contour map in Fig. 5a demonstrates the variation of peak cooling load reduction with λ and α. When λ is kept constant, an increase in α decreases the peak cooling load. However, when α is also kept constant, excessively high thermal conductivity reduces the potential for peak cooling load reduction. Too low thermal conductivity will also have adverse effects on peak cooling load reduction due to the inability of the material to absorb and release heat. Materials positioned closer to the upper right corner of the contour map can meet higher indoor cooling demand requirements with less material usage.

The amount of heat absorbed by internal thermal mass during daytime is influenced not only by the inherent thermal properties of the materials but also by the thickness. Thickness varying from 0 and 17 mm at an interval of 3.40 mm is selected to derive the optimum size of internal thermal mass for reducing daily cooling demand. For all the six selected materials, the total cooling effect increases with the increase of thermal mass thickness before reaching an optimum thickness (Fig. 5b), that is between 28 mm and 45 mm. After the optimum thickness is reached, the total absorbed heat will decline. When the thickness is smaller than the optimum value, internal thermal mass acts as a source to release heat at night and a sink to absorb heat at day. Once the thickness is beyond the optimum value, internal thermal mass acts as a large source keeping absorbing heat at night and day. Among the six selected materials, concrete has the smallest optimum thickness of 28 mm and the total absorbed heat from room air declines most rapidly with increasing thickness after the threshold is achieved. The rate of this decline in the total absorbed heat is related to the thermal diffusivity. Higher thermal diffusivity leads to a faster decline.

3.3. Envelop configuration

Envelope configurations affect the efficiency of nighttime natural

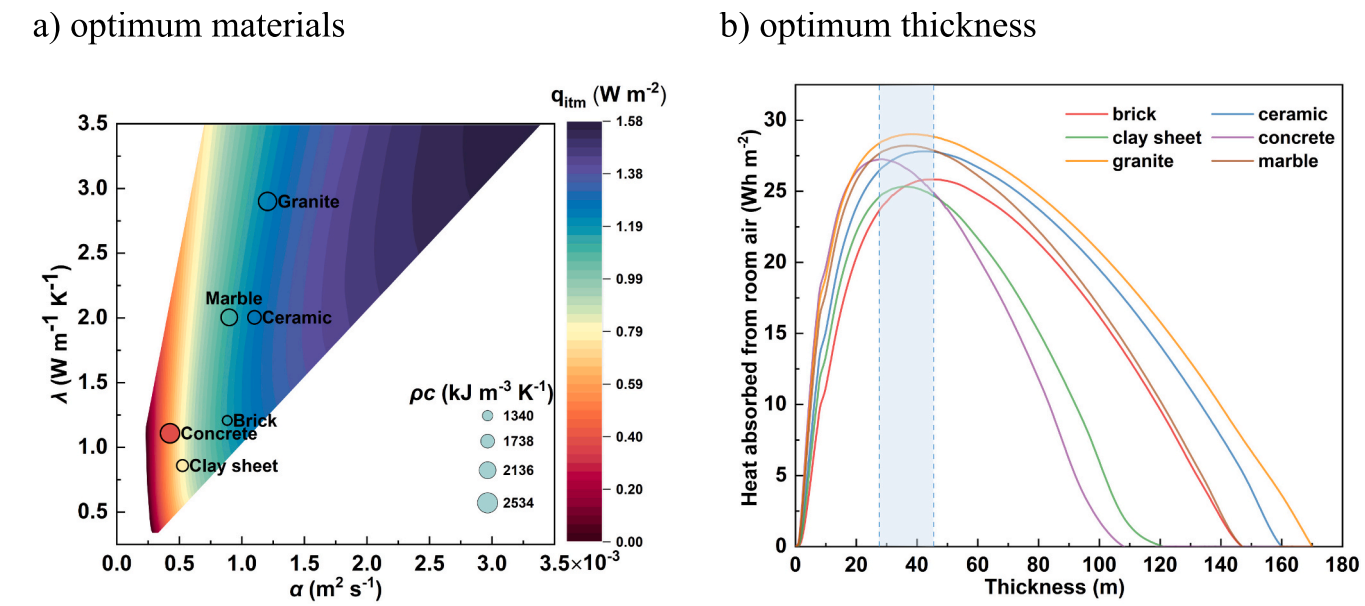

Fig. 5. (a) Peak cooling load reduction potential of different materials in Taos, New Mexico, in July; bubble size represents the heat capacity of the thermal mass; (b) variation of total heat absorbed from room air during the daytime with the material thickness.

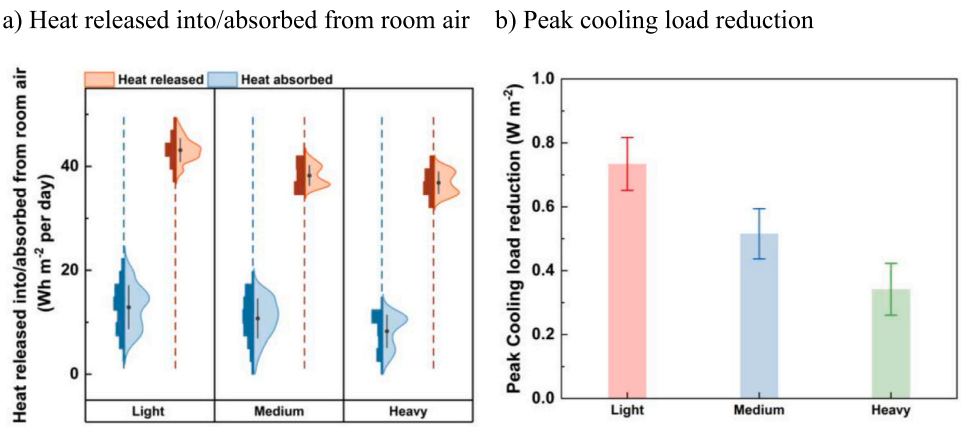

Fig. 6. (a) Total heat absorbed from room air and released into room air during the day and night under different envelope constructions, respectively; (b) peak cooling load reduction under different envelope constructions.

ventilation of internal thermal mass to a certain extent (Fig. 6), with granite being used as the thermal mass material. For all configurations, total heat released into room air at night is higher than the total heat absorbed from room air during the day. Only about 22–30% of total heat released at night is utilised to compensate the daytime cooling demand (Fig. 6a). For example, in lightweight buildings, internal thermal mass releases 43 ± 2.2 Wh m^{-2} of heat at night and absorbs only 15 ± 4.2 Wh m^{-2} of heat during the day. During the nighttime, only the top part of the internal thermal mass is cooled. Therefore, during the daytime, the top part absorbs heat from both the room and the bottom part of the internal thermal mass. This leads to the nonequilibrium of the thermal mass. Compared to lightweight structures, medium- and heavyweight construction results in an 11.1% and 14.4% decrease in the total amount of released heat, respectively. This is because heavyweight structures further delay the release of the daily absorbed heat, causing higher nighttime indoor air temperature that reduces the cooling effectiveness. On the other hand, medium- or heavyweight envelopes have a limited effect on total absorbed heat during the day. The total heat absorbed from room air is 11 ± 3.8 Wh m^{-2} and 8.3 ± 3.1 Wh m^{-2} per design day, respectively, for medium- and heavyweight buildings. During the daytime, the air conditioning system is used to maintain a constant room air temperature, reducing the influence of envelope configurations on the heat absorption process. However, the range of the total absorbed heat from room air is 2–13 Wh m^{-2} for different heavyweight envelopes, which is narrower than the range of 4–22 Wh m^{-2} for different lightweight envelopes.

Envelope configuration also affects the ability of internal thermal mass to reduce peak cooling load (Fig. 6b). In lightweight buildings, nighttime natural ventilation of internal thermal mass can reduce peak cooling load by 0.78 ± 0.35 W m^{-2}. On average, the peak cooling load reduction in medium- and heavyweight buildings, is 67% and 44%, respectively, of that in lightweight buildings. A combination of lightweight envelops and internal thermal mass shows a better performance on cooling load reduction.

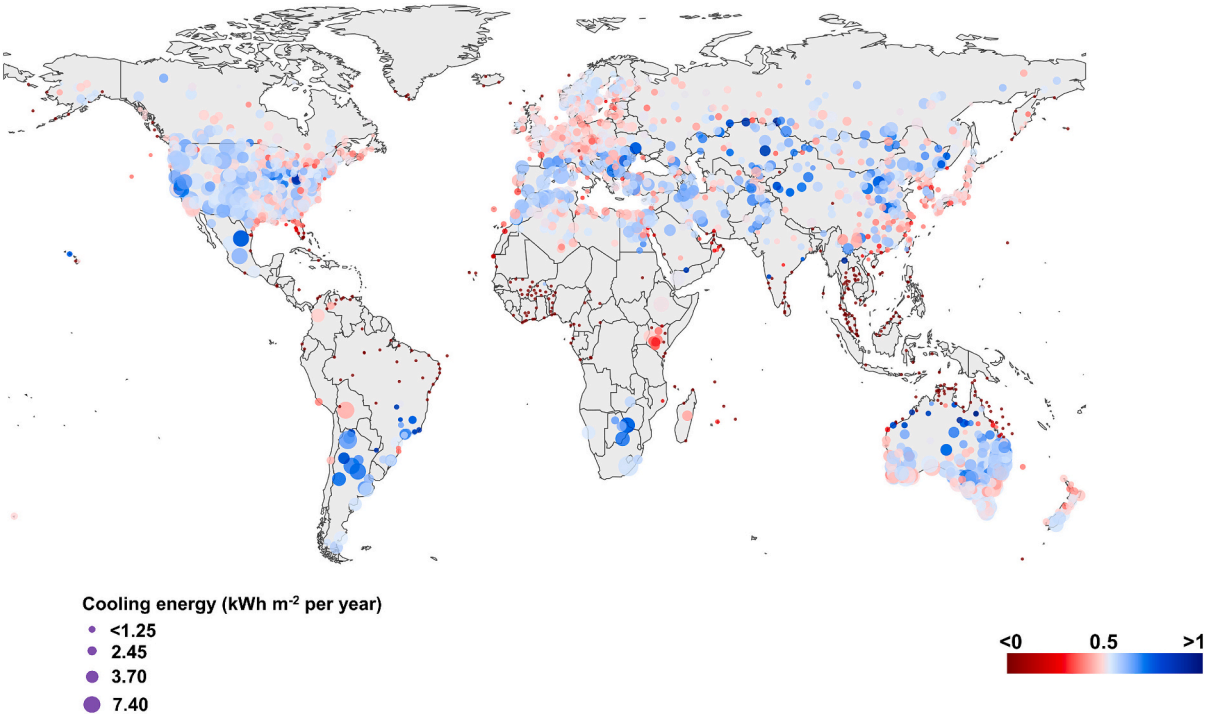

Fig. 7. Cooling demand reduction of nighttime natural ventilation of internal thermal mass in different climate zones. Bubble size represents the total heat absorbed from air and colour shows the ratio of absorbed heat to released heat.

3.4. Climate zones

There are two belts suitable for nighttime natural ventilation of internal thermal mass, locating between the Tropic of Cancer and 60 degrees north latitude, and between the Tropic of Capricorn and 45 degrees south latitude (Fig. 7). The annual cooling demand reduction exceeds 1.25 kWh m^{-2} in these two belts. In comparison, the potential for nighttime natural ventilation near the equator is almost negligible. This is primarily because regions near the equator fall under tropical climate categories in the Köppen climate classification, in which there is minimal seasonal variation in temperatures, and the coldest month typically has an average temperature exceeding 18°C. For example, Jakarta, the capital of Indonesia, according to the ASHRAE 2021 Handbook, the design temperature in this region remains above 27.7°C throughout the year, with an average annual design wind speed of 1.4 m s^{-1}. Consequently, the small diurnal temperature variation and low nighttime wind speeds pose significant challenges for the absorption and release of heat through internal thermal mass.

In polar or subpolar climate zones, a scarce data distribution in high-latitude regions such as northern Canada and Greenland, hinders incomplete quantification of nighttime natural ventilation in these regions. This situation is primarily because of extremely low population density and lack of meteorological stations. Moreover, the existing ASHRAE design-month weather data miss necessary wind speed for these regions. Due to phenomena like polar day and polar night, there is also an absence of Clear Sky Solar Irradiance data. Therefore, calculation has not been performed for these regions.

Desert climates exhibit an extraordinary potential for nighttime natural ventilation of internal thermal mass throughout the year (Table 3). Among the selected desert areas, the minimum annual cooling demand reduction is 2.01 kWh m^{-2} in Arabian Desert and the maximum annual cooling demand reduction reaches 6.67 kWh m^{-2} in Mojave Desert. In Kalgoorlie, Australia, the annual cooling demand reduction can reach 4.98 kWh m^{-2}. In Saltillo, Mexico, the annual cooling demand reduction can reach 6.33 kWh m^{-2}. Elevated cooling potentials in desert areas are due to high daily temperature range, low humidity, and intense wind. The year-round average of the design wind speed in Kalgoorlie, Australia is 4 m s^{-1}, and the average daily temperature range is 12.7°C. The large diurnal temperature differences and high wind speeds provide optimal conditions for nighttime natural ventilation of internal thermal mass.

Within the temperate climate zone including Europe, the eastern United States, southeastern Latin America, New Zealand, and the southern regions of China, the average cooling demand reduction is about 2.45 kWh m^{-2} per year. The low efficiency of applying nighttime natural ventilation of internal thermal mass is discerned. The red bubbles indicate less than 50% of the total heat released from thermal mass has been utilised at day. This is primarily due to the distinct seasonal variations in these regions, featuring with relatively low diurnal temperature differences. But regions near the ocean in temperate zones are particularly suitable for applying the nighttime natural ventilation of internal thermal mass. The cooling demand reduction per year can reach 5.79 kWh m^{-2} in Dunedin (New Zealand), 5.25 kWh m^{-2} in Rozas (Spain), 4.85 kWh m^{-2} in Viedma (Argentina), 4.77 kWh m^{-2} in North Carolina (USA), etc.

Table 3
Cooling demand reduction in selected desert areas.

Dessert	Regions	Absorbed Heat(kWh m^{-2})
Arabian Desert	Dammam	2.01
	Hail	4.13
Chihuahuan Desert	Santa Fe	6.06
Gobi Dessert	Tikanlik	3.46
	Tongde	3.26
Great Basin Desert	Reno	5.94
Great Victoria Desert	Kalgoorlie	4.98
	Coober Pedy	2.92
Karakum Desert	Ashgabat	2.49
	Mary	2.62
Mojave Desert	Edwards AFB	6.67
Namib Desert	Walvis Bay	5.13
	Keetmanshoop	2.36
Sahara Desert	Ajdabiya	3.61
	Baharia	3.39
Thar Desert	Sri Ganganagar	2.61
	Batman	3.16

3.5. Further discussions

Above analysis of cooling demand reduction uses the design-day weather profiles. To understand if the outcomes are still valid under real-world hourly-varied weather profiles, the cooling demand reduction is compared for the two profiles in April in Taos (Fig. 8a). The percentage errors between the actual and design month data for heat absorption and release are 4.65% and 7.66%, respectively, demonstrating the reliability of using design-day weather data for the analysis. The analysis of the optimum materials for internal thermal mass, material thickness and the impact of envelop configurations is confined to the hottest month – July in Taos, New Mexico. As it is expected that internal thermal mass would function better in other summer and transitional seasons if it works in the hottest month. This seasonal effect is further explored for Taos from April to October (Fig. 8b). The total heat released and absorbed is inversely related to the corresponding monthly design temperature. In the hottest month July, the total absorbed heat is 8.3 Wh m^{-2}, which increases to 48.8 Wh m^{-2} in October and 55.5 Wh m^{-2} in April. The difference in the design outdoor temperature is only 1.7°C between October and April. The wind speed is 4.1 m s^{-1} in April and 1 m s^{-1} larger than that in October, indicating that wind speed becomes a secondary but critical factor influencing the cooling demand reduction when monthly design temperatures and daily ranges are nearly identical. To further explore the effect of daily range in the hottest month and annual wind speed, the distribution of these two parameters for regions with absorbed heat over 3.70 kWh m^{-2} and less than 1.25 kWh m^{-2} is compared in Fig. 9. The impact of DBR and wind speed is obtained from simulation results. The calculated cooling demands are stored in a table containing the city name, latitude, longitude, and weather data. Based on the calculated annual cooling demand values, the selected sample regions are classified into four categories. For each category, statistical values of DBR and wind speed are retrieved. The average of the daily range is 12.6°C in the regions of cooling demand reduction over 3.70 kWh m^{-2}, about 5.7°C higher than that in the region of cooling demand reduction less than 1.25 kWh m^{-2}. Conversely, the annual wind speed is 3.21 m s^{-1} in the regions of cooling demand reduction over 3.70 kWh m^{-2}, 0.98 m s^{-1} smaller than that in the region of cooling demand reduction less than 1.25 kWh m^{-2}. It indicates that the daily range is the predominate factor comparing to wind speed.

The above analysis of optimum materials considered only cooling demand reduction. To identify materials that are also cost-effective, an economic analysis was conducted using Taos as a case study (Fig. 10). The cost of materials, lifespan, salvage value, and methods for calculating annualized costs are detailed in Appendix C. An interest rate of 4.8% was applied. The net present value (NPV) based on material prices is significantly lower than the NPV based on material lifespan, indicating that the NPV of materials is more influenced by their lifespan. Since brick has a lower average price compared to other materials and a lifespan of about 100 years, it results in the lowest annualized cost of 0.035 USD m^{-2}. Although concrete has a lower average price, its shorter average lifespan of about 15 years leads to the highest annualized cost. Granite, with its superior ability to reduce cooling load demand, performs best in terms of annual energy savings of 1.14 USD m^{-2}, while concrete, due to its thermal properties, shows the weakest performance in reducing cooling load demand and consequently results in the lowest

a) Comparasion of design-day and real-world weather

b) Total heat absorbed from air and heat released into airin different months

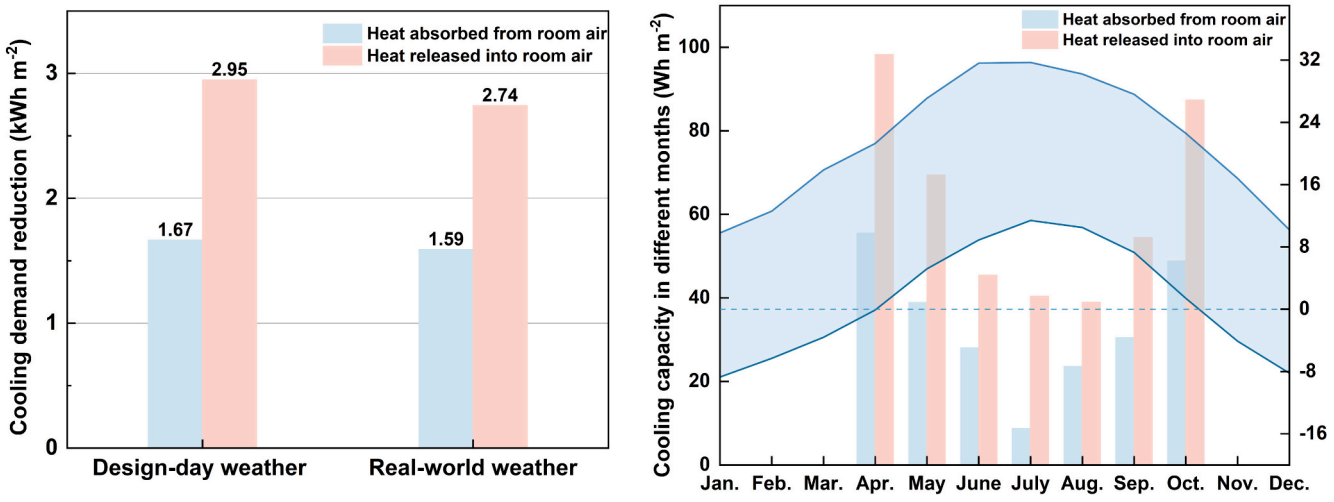

Fig. 8. (a) Comparison of monthly cooling demand reduction under design-day and hourly-varied weather profiles; (b) total heat absorbed from air and heat released into air during different months in Taos, New Mexico. The shaded region represents the daily range of monthly design temperature.

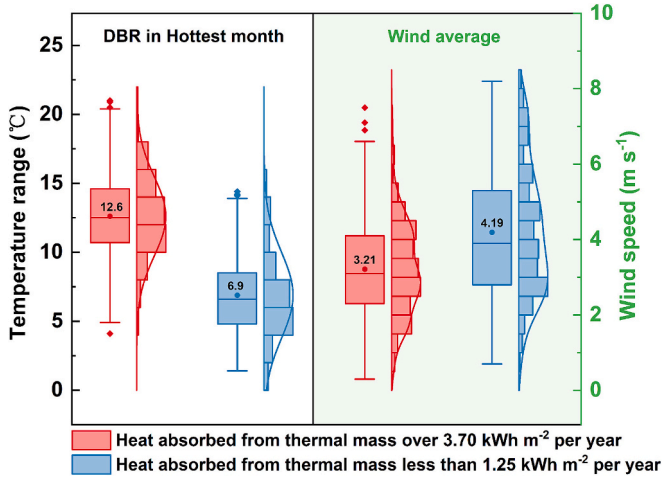

Fig. 9. Comparison of DBR in hottest month and annual wind average over suitable and general regions using nighttime natural ventilation of internal thermal mass.

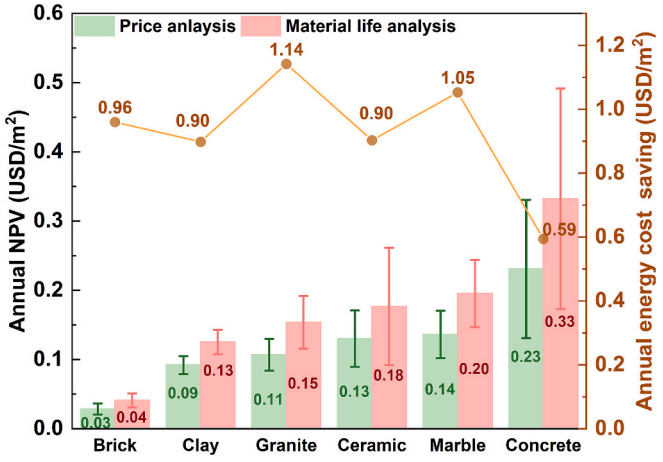

Fig. 10. Economic analysis of different internal thermal mass materials in Taos.

annual energy savings of 0.59 USD m^{-2}. Considering both the annualized cost and annual energy savings, brick and granite emerge as suitable materials due to their lower NPV and higher energy cost savings.

4. Conclusions

The research on nighttime natural ventilation of internal thermal mass is limited due to lacking a design tool. This study develops such a modelling framework and validates the mathematical model for internal thermal mass by experiments in a climate chamber. A relative error of 0.27%–6.83% in surface temperatures shows a good agreement between experiments and the model. The modelling framework is further used to quantify the cooling demand reduction with different materials for internal thermal mass in buildings with varied envelop configurations in different climate zones. Following conclusions are drawn:

1) The optimum materials of nighttime natural ventilation of internal thermal mass among six potential materials is granite, due to large thermal mass of 2385 kJ m^{-3} $K^{-1}$and high thermal conductivity of 2.9 W m^{-1} K^{-1}. Using granite can result in peak cooling load reduction by about three times more effective than concrete. A sensitivity analysis contour map shows the variation of peak cooling load reduction with thermal conductivity and thermal diffusivity. The optimum thickness for six selected materials is between 28 mm and 45 mm, and concrete has the smallest optimum thickness of 11 mm, due to the high thermal diffusivity.
2) The combination of lightweight construction with internal thermal mass shows better performance, with internal thermal mass releasing 43 ± 2.2 Wh m^{-2} of heating at night, 11.1% and 14.4% more than that in medium- and heavyweight construction, because heavyweight envelop could further delay the release of the daily absorbed heat. On the other hand, the absorbed heat of thermal mass in lightweight envelops is 15 ± 4.2 Wh m^{-2} per design day, 16.7% and

35.9% higher than that in medium- and heavyweight construction, respectively.

3) The two belts between the Tropic of Cancer and 60 degrees north latitude, and between the Tropic of Capricorn and 45 degrees south latitude are the suitable regions for nighttime natural ventilation of internal thermal mass, where the annual cooling demand reduction exceeded 1.23 kWh m^{-2}. In different climate zones, dessert climate zone exhibits extraordinary potential for cooling demand reduction, such as Edwards AFB, which reaches up to 6.67 kWh m^{-2} of annual absorbed heat due to the high daily temperature range, low humidity, and intense wind. Temperate climate zone shows a low efficiency, due to the relatively low diurnal temperature difference, but regions near the ocean such as Dunedin, New Zealand can reach a cooling load reduction up to 5.79 kWh m^{-2} per year. Through the analysis of weather data from suitable and general regions, it has been determined that temperature range is the predominant factor influencing the performance of cooling demand reduction, in comparison to wind speed.

CRediT authorship contribution statement

Mingtong Li: Writing – original draft, Visualization, Validation, Software, Methodology, Investigation, Data curation. **Xiong Shen:** Writing – review & editing, Formal analysis. **Wentao Wu:** Writing – review & editing, Writing – original draft, Supervision, Resources, Methodology, Funding acquisition, Conceptualization. **Kristen Cetin:** Writing – review & editing, Supervision. **Finn Mcintyre:** Writing – review & editing, Resources. **Liangzhu Wang:** Writing – review & editing, Supervision. **Lixing Ding:** Writing – review & editing. **Daniel Bishop:** Writing – review & editing. **Larry Bellamy:** Writing – review & editing. **Meng Liu:** Writing – review & editing, Supervision.

Declaration of competing interest

The authors declare that they have no known competing financial interests or personal relationships that could have appeared to influence the work reported in this paper.

Acknowledgement

Dr. Wu would like to acknowledge the support of the Royal Society New Zealand through the Catalyst Seeding General grant with Reference Number: 22-UOC-008-CSG.

Appendix A. Review of external thermal mass on reduction of energy / overheating hours

Table A1
External thermal mass on reduction of energy /overheating hours.

Ref.	Climate zone	Building type	T_o	*Software*	T_{set}	Thermal mass material	Energy/ Overheating hours reduction
[6]	temperate	Lightweight/ Heavyweight	$T_{o,avg} = 24.8$ °C	Abaqus CAE 6.12–2	26 °C	Timber/ Blockwork	–
[9]	temperate	Lightweight/ Heavyweight	$T_{o,avg} = 24.9$ °C	–	25 °C–26 °C	Sand block/ cellular concrete	67 %–75 %
[10]	cold-humid	Heavyweight	Variable regions	RC, EnergyPlus	21.2 °C–23.9 °C	Concrete	20 % - 75 %
[11]	hot desert	Mediumweight	$T_{o,min} = 28.6$ °C $T_{o,max} = 35.2$ °C	TRNSYS 17	–	Stone	72 %
[12]	hot	Heavyweight	$T_{o,avg} = 35$ °C	FEM, COMSOL Multiphysics	26 °C	Concrete	3 kWh m^{-2} per year
[13]	temperate	Heavyweight	–	EnergyPlus	–	Concrete	−17.5 %

Appendix B. Derivation of the analytical model

The temperature field in internal thermal mass is described by the following equation with Robin boundary conditions:

$$\rho c \frac{\partial T_x}{\partial t} = \frac{\partial^2 T_x}{\partial x} \tag{B1}$$

$$-\lambda A \left.\frac{\partial T_x}{\partial x}\right|_{x=L} = h(t) A [T_x(x = l, t) - T_r(t)] \tag{B2}$$

$$\left.\frac{\partial T_x}{\partial x}\right|_{x=0} = 0 \tag{B3}$$

$$T_x(x, 0) = T_r(0) \tag{B4}$$

Eq. (B1) described one-dimensional heat conduction in the internal thermal mass, x is the vertical distance from the bottom of the internal thermal mass (m), respectively. Eq. (B2) describes the heat exchange between the internal thermal mass and room air temperature T_r (K). The details of time varied T_r equation could be found in [18]. h is the hourly varied convection heat transfer coefficient and can be described using the step function:

$$h(t) = [H(t) - H(t - t_1)]\, h_1 + [H(t - t_1) - H(t - t_2)]\, h_2 + \cdots + [H(t - t_{m-2}) - H(t - t_{m-1})]\, h_{m-1} + H(t - t_{m-1}) h_m \tag{B5}$$

$$H(t) = \begin{cases} 0 & t \le 0 \\ 1 & t > 0 \end{cases} \tag{B6}$$

For ease of calculation, we normalize T_x, x, h, T_r as:

$$\theta = \frac{T_x - T_r(0)}{T_r(0)} \tag{B7}$$

$$\eta = \frac{x}{l} \tag{B8}$$

$$Bi = \frac{hL}{\lambda} \tag{B9}$$

$$\theta_r = \frac{T_r - T_r(0)}{T_r(0)} \tag{B10}$$

The Eqs. (B1-B4) can be normalized as:

$$\frac{\partial \theta}{\partial t} = \frac{\alpha}{l^2}\frac{\partial^2 \theta}{\partial \eta^2} \tag{B11}$$

$$-\frac{\partial \theta}{\partial \eta} = Bi\,(\theta - \theta r)\Big|_{\eta=1} \tag{B12}$$

$$\left.\frac{\partial \theta}{\partial \eta}\right|_{\eta=0} = 0 \tag{B13}$$

$$\theta(\eta, 0) = \theta r(0) = 0 \tag{B14}$$

The shifting function method is used to solve Eq. (B11) under the inhomogeneous Robin boundary condition given by Eq. (B12):

$$\theta(\eta, t) = \Psi(\eta, t) + u(t)v(\eta) \tag{B15}$$

where $v(\eta)$ is a shifting function and $u(\tau)$ contains time-dependent boundary values. To ensure the homogeneity of the Robin boundary condition, u and v followed by eq. (B17–18), and the solution through separation of variables followed by eq. (B19)

$$\frac{\partial \Psi}{\partial t} + v\frac{du}{dt} = \frac{\alpha}{l^2}\left(\frac{\partial^2 \Psi}{\partial \eta^2} + u\frac{d^2 v}{d\eta^2}\right) \tag{B16}$$

$$u = Bi\theta r \tag{B17}$$

$$v = \frac{\eta^2 - 1}{2} \tag{B18}$$

$$\frac{\partial \Psi}{\partial t} = \frac{\alpha}{l^2}\frac{\partial^2 \Psi}{\partial \eta^2} + Bi\theta r - \frac{1}{2}Bi\left(\eta^2 - 1\right)\frac{d\theta r}{dt} \tag{B19}$$

Eq. (B19) can be separated into variables again, resulting in Eq. (B20). One term is handled using the Fourier transform (B21), while the other term is solved by applying the variation of parameters (VOP) method and the principle of orthogonality (B23), under the assumption of an initial condition of zero, leading to Eqs. (B24–B30).

$$\Psi(\eta, t) = \varphi(t)\varepsilon(\eta) \tag{B20}$$

$$\varepsilon = cos(\beta_n \eta) \tag{B21}$$

$$R_n = \frac{\beta_n^2 + {Bi_0}^2 + Bi_0}{2\left(\beta_n^2 + {Bi_0}^2\right)} \tag{B22}$$

$$\varphi_n = \frac{1}{R_n}\int_0^1 \Psi cos(\beta_n \eta) d\eta \tag{B23}$$

$$\frac{d\varphi_n}{dt} + p(t)\varphi_n = q(t) \tag{B24}$$

$$p(t) = \frac{\frac{\alpha}{l^2}\left(\beta_n^2 + S2_n B\right) - S4_n \dot{B}}{1 - S4_n B} \tag{B25}$$

$$q(t) = \frac{\frac{\alpha}{l^2} Bi\theta_r - S3_n\left(Bi\dot{\theta}_r + \dot{B}i\theta_r\right)}{1 - S4_n B} \tag{B26}$$

$$S1_n = \frac{sin\beta_n}{R_n \beta_n} \tag{B27}$$

$$S2_n = S1_n cos\beta_n \tag{B28}$$

$$S3_n = \frac{cos\beta_n}{R_n\beta_n^2} - \frac{sin\beta_n}{R_n\beta_n^3} \tag{B29}$$

$$S4_n = S3_n cos\beta_n \tag{B30}$$

$$W1_{j+1,n} = S1_n Bi_{j+1}\theta r_{j+1} \tag{B31}$$

$$W2_{j+1,n} = \frac{\beta_n^2 + S2_n B_{j+1}}{1 - S4_n B_{j+1}} \tag{B32}$$

$$W3_{j+1,n} = S3_n\left(2Bi_{j+1}\theta_{rj+1} - Bi_{j+1}\theta r_j - Bi_j\theta r_{j+1}\right) \tag{B33}$$

$$W4_{j+1,n} = \left|1 - S4_n B_{j+1}\right| \tag{B34}$$

Appendix C. Details of economic analysis

In Taos, the annual cost calculation for the NPV of internal thermal mass made from different materials is conducted using Eq. (C1), while future electricity price growth rates are estimated by fitting the commercial electricity rates for 2023–2024 using Eq. (C2). The cost of materials, lifespan, and salvage value of the materials are shown in Table C1. By incorporating the annual energy savings in the region, the final annual energy cost savings are calculated with Eq. (C3):

$$C_a = \frac{1}{n}\sum_{n=1}^{n}\frac{C_c - C_{sal}}{n(1+c)^n} \tag{C1}$$

$$y(x) = 0.09x + 12.08 \tag{C2}$$

$$C_{sav} = \frac{1}{n}\sum_{n=1}^{n} E_{TM}y(x) \tag{C3}$$

where C_a is annual NPV, C_c is the cost of internal thermal mass material, C_{sal} is the salvage value of the specific material, n is the material life, c is the interest rate, C_{sav} is annual energy cost saving, and E_{TM} is annual energy saving amount.

Table C1
Investment parameters of materials.

Material	Price (USD m^{-2})	Material life (year)	Salvage Value (%)
Brick	8–20	100	1
Ceramic	5–15	20–50	0
Clay	10–15	50	0
Concrete	5–30	20–50	1
Granite	35–75	100	5
Marble	40–100	100	5

Data availability

Data will be made available on request.

References

[1] IEA. World energy outlook2023; 2023. IEA, Paris.
[2] Jalali Z, Shamseldin AY, Ghaffarianhoseini A. Urban microclimate impacts on residential building energy demand in Auckland. New Zealand: A climate change perspective, Urban Clim 2024;53:101808. https://doi.org/10.1016/j.uclim.2024.101808.
[3] Lo SH, Chen CT, Hsu HH, Shih MF, Liang HC. The unprecedented spatial extent and intensity of the 2021 summer extreme heatwave event over the Western north American regions. Weather Clim Extrem 2023;41:100576. https://doi.org/10.1016/J.WACE.2023.100576.
[4] Reuters. Arizona power demand breaks records during heatwave. 2023. https://www.reuters.com/business/energy/arizona-power-demand-breaks-records-during-heatwave-2023-07-18/#:~:text=The peak demand of 8%2C191,in a release on Monday.
[5] Li Y, Tao X, Zhang Y, Li W. Combining use of natural ventilation, external shading, cool roof and thermal mass to improve indoor thermal environment: field measurements and simulation study. J Build Eng 2024;86:108904. https://doi.org/10.1016/j.jobe.2024.108904.
[6] Reilly A, Kinnane O. The impact of thermal mass on building energy consumption. Appl Energy 2017;198:108–21. https://doi.org/10.1016/J.APENERGY.2017.04.024.
[7] Lind J, Möllerström E, Averfalk H, Ottermo F. Energy flexibility using the thermal mass of residential buildings. Energy Build 2023;301. https://doi.org/10.1016/j.enbuild.2023.113698.
[8] Samini MA, Hashemi A, Asgari A. The impact of thermal mass on envelope heat loss in the caldarium of Yazd's traditional baths. Results Eng 2024;22:102266. https://doi.org/10.1016/j.rineng.2024.102266.
[9] Kuczyński T, Staszczuk A. Experimental study of the influence of thermal mass on thermal comfort and cooling energy demand in residential buildings. Energy 2020;195. https://doi.org/10.1016/j.energy.2020.116984.
[10] He Y, Zhou H, Fahimi F. Modeling and demand-based control of responsive building envelope with integrated thermal mass and active thermal insulations. Energy Build 2022;276:112495. https://doi.org/10.1016/j.enbuild.2022.112495.
[11] Mousa WAY, Lang W, Yousef WA. Simulations and quantitative data analytic interpretations of indoor-outdoor temperatures in a high thermal mass structure. J Build Eng 2017;12:68–76. https://doi.org/10.1016/j.jobe.2017.05.007.
[12] Alayed E, Bensaid D, O'Hegarty R, Kinnane O. Thermal mass impact on energy consumption for buildings in hot climates: a novel finite element modelling study comparing building constructions for arid climates in Saudi Arabia. Energy Build 2022;271:112324. https://doi.org/10.1016/j.enbuild.2022.112324.
[13] Sun H, Calautit JK, Jimenez-Bescos C. Examining the regulating impact of thermal mass on overheating, and the role of night ventilation, within different climates and future scenarios across China. Clean Eng Technol 2022;9. https://doi.org/10.1016/j.clet.2022.100534.

[14] Dias B, Carrilho G. Using building thermal mass energy storage to offset temporary BIPV output reductions due to passing clouds in an office building207; 2022. https://doi.org/10.1016/j.buildenv.2021.108504.
[15] Antonopoulos KA, Koronaki EP. Effect of indoor mass on the time constant and thermal delay of buildings. Int J Energy Res 2000;24:391–402. https://doi.org/10.1002/(SICI)1099-114X(200004)24:5<391::AID-ER585>3.0.CO;2-L.
[16] Johra H, Heiselberg P, le Dréau J. Influence of envelope, structural thermal mass and indoor content on the building heating energy flexibility. Energy Build 2019;183:325–39. https://doi.org/10.1016/J.ENBUILD.2018.11.012.
[17] ASHRAE Technical Committee. In: ASHRAE terminology of heating, ventilating, air conditioning, and refrigeration; 2024.
[18] Wu W, Benner J, Luo Z. Developing analytical model for nighttime cooling of internal thermal mass. Appl Therm Eng 2023;220. https://doi.org/10.1016/j.applthermaleng.2022.119798.
[19] Chenari B, Dias Carrilho J, Gameiro Da Silva M. Towards sustainable, energy-efficient and healthy ventilation strategies in buildings: a review. Renew Sust Energ Rev 2016;59:1426–47. https://doi.org/10.1016/j.rser.2016.01.074.
[20] Zhang H, Yang D, Tam VWY, Tao Y, Zhang G, Setunge S, et al. A critical review of combined natural ventilation techniques in sustainable buildings. Renew Sust Energ Rev 2021;141:110795. https://doi.org/10.1016/J.RSER.2021.110795.
[21] Lança M, Coelho PJ, Viegas J. Numerical simulation of a night cooling strategy in an office room. Energy Build 2021;252:111359. https://doi.org/10.1016/j.enbuild.2021.111359.
[22] Albuquerque DP, Mateus N, Avantaggiato M, Carrilho da Graça G. Full-scale measurement and validated simulation of cooling load reduction due to nighttime natural ventilation of a large atrium. Energy Build 2020;224:110233. https://doi.org/10.1016/j.enbuild.2020.110233.
[23] Amaripadath D, Paolini R, Sailor DJ, Attia S. Comparative assessment of night ventilation performance in a nearly zero-energy office building during heat waves in Brussels. J Build Eng 2023;78:107611. https://doi.org/10.1016/j.jobe.2023.107611.
[24] Li X-X, Huang K-L, Feng G-H, Li W-Y, Wei J-X. Night ventilation scheme optimization for an ultra-low energy consumption building in Shenyang, China. Energy Reports 2022;8:8426–36. https://doi.org/10.1016/j.egyr.2022.06.059.
[25] Kuczyński T, Staszczuk A, Gortych M, Stryjski R. Effect of thermal mass, night ventilation and window shading on summer thermal comfort of buildings in a temperate climate. Build Environ 2021;204:108126. https://doi.org/10.1016/j.buildenv.2021.108126.
[26] Gagliano A, Nocera F, Patania F, Moschella A, Detommaso M, Evola G. Synergic effects of thermal mass and natural ventilation on the thermal behaviour of traditional massive buildings. Int J Sustainable Energy 2016;35:411–28. https://doi.org/10.1080/14786451.2014.910517.
[27] Yoon N, Norford L, Wetter M, Malkawi A. Development of window scheduler algorithm exploiting natural ventilation and thermal mass for building energy simulation and smart home controls. J Build Eng 2024;82:108158. https://doi.org/10.1016/j.jobe.2023.108158.
[28] Oropeza-Perez I, Ostergaard PA. Energy saving potential of utilizing natural ventilation under warm conditions – a case study of Mexico. Appl Energy 2014;130:20–32. https://doi.org/10.1016/J.APENERGY.2014.05.035.
[29] Fan X, Li X. Performance comparison analysis for different single-zone natural ventilation building indoor temperature prediction method combined thermal mass. Energy 2022;255:124518. https://doi.org/10.1016/j.energy.2022.124518.
[30] Yu J, Lu Y, Hu J, Zhong K, Jia T, Yang X. Prediction models for building thermal mass of intermittently heated rooms for balancing energy consumption and indoor thermal comfort. Energy Build 2024;317:114376. https://doi.org/10.1016/j.enbuild.2024.114376.
[31] Lu Y, Yang Z, Yu J, Chen B, Zhong K. Development of a second-order dynamic model for quantifying impact of thermal mass on indoor thermal environment. J Build Eng 2021;42:102496. https://doi.org/10.1016/j.jobe.2021.102496.
[32] Askeland M, Georges L, Korpås M. Low-parameter linear model to activate the flexibility of the building thermal mass in energy system optimization. Smart Energy 2023;9:100094. https://doi.org/10.1016/j.segy.2023.100094.
[33] Mugnini A, Ramallo-González AP, Parreño A, Molina-Garcia A, Skarmeta AF, Arteconi A. Dynamic building thermal mass clustering for energy flexibility assessment: an application to demand response events. Energy Build 2024;308. https://doi.org/10.1016/j.enbuild.2024.114011.
[34] Ning B, Zhang M, Li J, Chen Y. A revised radiant time series method (RTSM) to calculate the cooling load for pipe-embedded radiant systems. Energy Build 2022;268:112199. https://doi.org/10.1016/J.ENBUILD.2022.112199.
[35] Larsen TS, Plesner C, Leprince V, Carrié FR, Bejder AK. Calculation methods for single-sided natural ventilation: now and ahead. Energy Build 2018;177:279–89. https://doi.org/10.1016/j.enbuild.2018.06.047.
[36] Yang L, Li Y. Cooling load reduction by using thermal mass and night ventilation. Energy Build 2008;40:2052–8. https://doi.org/10.1016/j.enbuild.2008.05.014.
[37] McQuiston FC, Parker JD. Heating, ventiling and air conditioning, analysis and design, sixth. New York: John Wiley and Sons; 1994.
[38] Beausoleil-Morrison I. The adaptive simulation of convective heat transfer at internal building surfaces. 2002. www.elsevier.com/locate/buildenv.
[39] Guo R, Heiselberg P, Hu Y, Johra H, Jensen RL, Jønsson KT, et al. Experimental investigation of convective heat transfer for night ventilation in case of mixing ventilation. Build Environ 2021;193:107670. https://doi.org/10.1016/J.BUILDENV.2021.107670.
[40] Energy performance of buildings - ventilation for buildings. 2017. in: ISO Standard EN 16798–7:2017, BSI Standars Limited 2017.
[41] Xie X, Luo Z, Grimmond S, Blunn L. Use of wind pressure coefficients to simulate natural ventilation and building energy for isolated and surrounded buildings. Build Environ 2023;230. https://doi.org/10.1016/j.buildenv.2022.109951.
[42] ASHRAE Research. ASHRAE handbook-fundamentals. 2021. p. 2021.
[43] Tatsidjodoung P, le Pierrès N, Luo L. A review of potential materials for thermal energy storage in building applications. Renew Sust Energ Rev 2013;18:327–49. https://doi.org/10.1016/J.RSER.2012.10.025.
[44] https://ashrae-meteo.info/v2.0/# ASHRAE CLIMATIC design conditions 2009/2013/2017/2021. 2021.
[45] Beck HE, Zimmermann NE, McVicar TR, Vergopolan N, Berg A, Wood EF. Present and future köppen-geiger climate classification maps at 1-km resolution. Sci Data 2018;5. https://doi.org/10.1038/sdata.2018.214.
[46] Tian Z, Zheng W, Guo J, Jiang Y, Liang Z, Mi X. Fundamental research on the condensation heat transfer of the hydrocarbon-mixture energy in a spiral tube described by a universal model using flow pattern based and general modes. Energy 2024;296:131019. https://doi.org/10.1016/J.ENERGY.2024.131019.